INSTALLED PERFORMANCE OF AIR-AUGMENTED NOZZLES BASED ON ANALYTICAL DETERMINATION OF INTERNAL EJECTOR CHARACTERISTICS

by

Helmut H. Korst, Alva L. Addy, W. L. Chow
Department of Mechanical and Industrial Engineering
University of Illinois, Urbana, Illinois

ABSTRACT

The basic idea of air augmentation is to take aboard atmospheric air and let it interact with the primary propulsive stream before or while discharging through the ejector nozzle. This idea suggests that one has to be concerned not only with an ejector problem, but also with the aerodynamics of intakes, the flow past boattails, and the jet-slip-stream interaction near the exit of the ejector.

The recent development of analytical methods for dealing with the ejector problem now makes it possible to propose and exploit quantitatively an entirely theoretical flow model for evaluating in-flight performance of vehicle-integrated air-augmented propulsion systems.

The theoretical ejector flow model can cope with a wide range of practical shroud configurations (especially with non-cylindrical contours) and with three basic types of primary-secondary stream interaction, namely, inviscid, viscid (energy transfer), and reactive (afterburning along fuel-rich rocket exhaust gas surface).

In this paper, procedures for matching intake and ejector pumping characteristics are outlined for either experimentally or theoretically available intake performance information. In addition, the influence of external aerodynamics such as flow over the boattail and its interaction with the internal ejector performance are considered.

The present method is illustrated by applying the theoretical analysis to an air-augmented jet engine model investigated by NACA. Excellent agreement between theoretical and experimental data is obtained for static operation; in addition, the theoretical model also allows to predict analytically the in-flight performance of the ejector nozzle configuration.

1. INTRODUCTION

The potential of air augmentation to improve the installed performance of propulsive jets has received widespread attention and numerous experimental as well as theoretical investigations have been conducted to explore its utilization.

While the conceptual merits of air augmentation appear to be undisputed for vehicles whose trajectories remain within the atmosphere[1], the practical implementation of the principle, controlled by net thrust and gross weight considerations, often indicates only marginal, if any, improvement[2].

Therefore, it becomes evident that not a sweeping appraisal of a scheme but only a detailed analysis of entire systems under flight conditions based on the action and interaction of well understood basic mechanisms can lead to an understanding and evaluation of the true possibilities of air augmentation.

The basic idea of taking aboard atmospheric air and letting it interact with the primary propulsive stream before or while discharging through the ejector nozzle suggests that we have to be concerned not only with an ejector problem, but also with the aerodynamics of intakes, the flow past boattails, and the jet-slip-stream interaction near the exit of the ejector.

Although both experimental and analytical investigations have had their share in contributing to our knowledge of such component flow problems, the recent development of analytical methods for dealing with the ejector problem[3,4] now makes it possible to propose, and exploit quantitatively, an entirely theoretical flow model for evaluating in-flight performance of vehicle-integrated air-augmented propulsion systems.

2. SYSTEMS DEFINITION AND DELINEATION OF THRUST FORCE CONTRIBUTIONS

Each system is identified by a control domain within prescribed boundaries. Its

individual performance characteristics are obtained by utilization of the momentum principle and the theoretical determination of surface integrals by analysis of the flow processes within the system.

2.1 Ejector

The identifying control domain and the control surface utilized for the ejector analysis are shown in Figure 1.

The theoretical analysis of the flow problem within this domain yields information on the pumping characteristics and the pressure and shear stress distributions over the internal ejector shroud surface. This, in turn, allows determination of the Gross Thrust Force.

$$\bar{F}_{Gross} = \int_{E_{CP}} (P-P_\infty)\, d\bar{S}_E + \int_{E_{CP}} \rho \bar{V} (\bar{V} \cdot d\bar{S}_E) + \int_{E_{CS}} (P-P_\infty)\, d\bar{S}_E$$

$$+ \int_{E_{CS}} \rho \bar{V} (\bar{V} \cdot d\bar{S}_E) + \int_{E_{SH}} (P-P_\infty)\, d\bar{S}_E \qquad (1)^*$$

2.2 Intake

The identifying control domain and control surface utilized in the intake analysis are shown in Figure 2. The objective of the intake analysis (see section 3.2) is the determination of the thrust force contributions of the surfaces I_{SH} ($\bar{F}_{I_{SH}}$), I_R ($\bar{F}_{I_R}$) and the internal drag forces ($\bar{F}_{OB}$) as may be caused by structural elements (struts) or vortex generators.

Figure 2 also draws attention to the so-called "additive intake drag" which has to be accounted for when intake forces are to be determined on the basis of momentum flux integrals. Application of the momentum principle yields here

$$\bar{F}_{I_A} + \bar{F}_{I_R} + \bar{F}_{I_{SH}} + \bar{F}_{I_{OB}} = - \int_{I_{C1}} (P-P_\infty)\, d\bar{S}_I - \int_{I_{C1}} \rho \bar{V} (\bar{V} \cdot d\bar{S}_I) -$$

$$\int_{I_{C2}} (P-P_\infty)\, d\bar{S}_I - \int_{I_{C2}} \rho \bar{V} (\bar{V} \cdot d\bar{S}_I) \qquad (2)$$

---

* Note that the pressure integral extended over wall surfaces should be interpreted as including viscous stresses as well as hydrostatic pressures.

2.3 Entire Propulsive System

2.3.1 Afterbody

The identifying control domain and control surface utilized in the determination of the NET AFTERBODY THRUST FORCE are shown in Figure 3.

The overall system is obtained by joining the "ejector" and "intake" sub-systems along the now internal surfaces E_{CS} and I_{C2} and by considering, in addition, the boattail surface (and force $\bar{F}_B$).

The result obtained is:

$$\bar{F}_{Net} = \bar{F}_{Gross} - \bar{F}_{I_A} + \bar{F}_B - \int_{I_{C1}} (P-P_\infty)\, d\bar{S}_I - \int_{I_{C1}} \rho \bar{V}\, (\bar{V} \cdot d\bar{S}_I) \qquad (3)$$

Since the net afterbody thrust force can also be represented by

$$\bar{F}_{Net} = \Sigma \bar{F}_{Shroud} + \bar{F}_{I_R} + \bar{F}_{I_{OB}} + \int_{E_{CP}} (P-P_\infty)\, d\bar{S}_E + \int_{E_{CP}} \rho \bar{V}\, (\bar{V} \cdot d\bar{S}_E) \qquad (4)$$

Where $\Sigma \bar{F}_{Shroud} = \bar{F}_{E_{SH}} + \bar{F}_{I_{SH}} + \bar{F}_B$

the true role of the "additive intake drag" force is readily recognized.

2.3.2 Systems Matching

2.3.2.1 Internal matching has to be accomplished along the surfaces E_{CS} and I_{C2} (see Figure 3) with respect to the velocity and pressure distributions.[1]

2.3.2.2 External matching has to be considered for surface E_{CE} (see Figure 1) for such combinations of external and internal flow conditions which would affect only the pressure distribution over the shroud (for choked ejector operation) or, in addition, the secondary mass flow through the ejector (for unchoked ejector operation).

---

[1] Actually, the matching procedure will remain restricted to the matching of integral values such as the secondary mass flow and a single representative secondary stagnation pressure.

2.3.3 Performance Evaluation

The ultimate purpose of the analysis is the evaluation of the net afterbody thrust under flight conditions and comparison with suitable reference thrust forces, such as the ideal convergent nozzle $F_{1D,C}$, or the ideal fully expanded nozzle F_{1D} (see section 4.3.4). Especially for rocket booster analysis, weight assessments have to be made in order to evaluate properly the merits of air-augmentation for specified (or optimized) trajectories[2].

The systems approach, as outlined above, provides for the formulation of performance characteristics of individual sub-systems and for their subsequent integration into the overall model. It is noteworthy that this can be achieved on a quantitative basis, and within a framework of simplifications which assure clarity in dealing with major design parameters without loss of essential features affecting the performance of flow components and the overall air-augmented system. In particular, simplifying assumptions will concern the nature of the secondary flow through the intake (complete uniformization of the intake flow prior to reaching the matching cross section I_{C2}) and through the ejector (one-dimensional annular flow inside of the ejector shroud, except for the dissipative regions of jet mixing and wall boundary layer. While the theoretical treatment of the ejector problem by itself would not necessitate such restrictions, it was felt that the matching procedure would become unduly complicated if rotational secondary flows were included.

In addition, the theoretical analysis of intakes will disregard the effect of additive drag and the influence of the intake flow on the boattail drag.

Flow over the boattail is excluded altogether from the evaluation of the net afterbody thrust force. Such information is readily available in the literature [5, 6] and since the only cases considered here are ones for which the ejector will operate entirely unaffected by the external flow field over the boattail, a detailed knowledge of the flow

past the boattail will not be required.

On the basis of these assumptions, the ejector analysis (given the ejector geometry and the stagnation states of the primary and secondary flows) will produce:

i) the pumping characteristics in the form of a simple $\frac{W_s}{W_p} = f(\frac{P_{os}}{P_{op}})$ relationship[3,4];

ii) the gross thrust, by integration of the stresses over the shroud.

A theoretical intake flow analysis (given the external flow approach conditions for both the free stream and the boundary layer configuration) will yield information of the type[7]: $\frac{P_{os}}{P_{o\infty}} = f(\frac{m}{m_\ell})$. Alternately, experimental investigation of specific intake configurations will produce information of the form: $\frac{P_{os}}{P_{o\infty}} = f(\frac{m}{m_o})$.

For any selected internal ejector performance point, items i) and ii) above, and afterbody operating conditions, the net afterbody thrust forces can be calculated for a variety of flight conditions by a suitable adaptation of well-known matching procedures for ejector and intake flows[9].

3. THEORETICAL ANALYSIS OF SYSTEM PERFORMANCE CHARACTERISTICS

3.1 Internal Ejector Performance

The ejector flow model is based on the inviscid and viscid interaction between the primary and secondary streams[3] within the confinement of generally non-cylindrical shrouds[4] with the additional consideration of the wall boundary layer. For the ejector operating in the supersonic regime[3], the secondary flow will generally reach a sonic condition inside of the shroud where the secondary flow area will be a minimum. In the analysis of this flow regime, the inviscid interaction is considered first, with viscous effects being introduced as a modification. Throughout the analysis, the secondary flow is assumed to sustain static pressures which are constant over its flow cross sections and continuous across the boundary of the primary stream.

3.1.1 Two-stream Inviscid Interaction

The primary flow field is determined by the method of characteristics while the secondary flow is assumed to be one-dimensional and reversible adiabatic. The secondary flow, for any chosen initial condition, is subject to a unique area-pressure relation, and such pressures are matched with the static pressures at the interface between the primary and secondary stream. The choking condition for the secondary stream in a minimum cross-sectional area within the shroud is determined by an iterative method which involves the entrance Mach Number of the secondary stream for a selected value of the stagnation pressure ratio.

Figure 4 shows schematically the inviscid flow configuration and notation while Table I lists the essential features of the computer program.[≠] According to Table I, given the ejector geometry and information concerning primary and secondary gas, the program produces information on the inviscid pumping characteristics and the static pressure distribution over the internal surface of the shroud. However, the effects of viscosity have yet to be considered.

3.1.2 Viscous Effects - Jet Mixing

Viscous interaction between the two streams occurs along their interface. This will result in:

i) a transfer of energy (shear work) from the primary to the secondary stream, and

ii) a modification of the pumping characteristics due to the displacement thickness of the mixing region.

Both effects are most pronounced for relatively small secondary flow rates, see Figure 5, where the theoretically calculated(inviscid and viscid) pumping characteristics of a divergent cooling-air ejector are compared with experimental data[10].

3.1.3 Viscous Effects - Shroud Wall Shear Layer

While the displacement effects due to the wall boundary layer are relatively insignificant, the shear stresses deserve attention since they tend to reduce the thrust, especially for relatively long shrouds. A computer program is available≠ which allows computation of boundary layer growth (including laminar-turbulent transition) in compressible flows with streamwise pressure gradients so that the loss of gross thrust due to friction can be determined.

3.1.4 Gross Thrust

Ultimately, on the basis of calculated internal ejector operating conditions, the gross thrust can be evaluated for a variety of static operating conditions of a divergent ejector. Figure 6 compares the results of our theoretical calculations with experimental data obtained by Huntley and Yanowitz[10].

3.1.5 Ejector Surface

For the purpose of the present analysis it has been assumed that the flow through the ejector was unaffected by the external flow field, or static pressure near the exit cross section.

A more complete picture of the internal operating characteristics and different operating regimes of an ejector system would be presented by the so-called "ejector surface"[3] (see figure 7).

Also indicated in Figure 7 is the geometric interpretation of matching between the ejector and intake as an intersection of their respective "operating surfaces".

3.2 Intake Performance

Examination of equation 2 in section 2.2 shows that the thrust force of the intake,

---

≠ For IBM 7094, Graduate College Department of Computer Science, University of Illinois.

$\bar{F}_{I_R} + \bar{F}_{I_{SH}} + \bar{F}_{I_{OB}}$, can be determined, with the exception of the unknown contribution of the additive drag, if the flow conditions in the cross sections I_{C1} and I_{C2} are known. A theoretical treatment of the intake flow problem[7] is based on the evaluation of the integrals over surfaces I_{C1} and I_{C2}. Such an analysis also yields information on the mass flow-pressure recovery relation, section 2.3.3, but introduces two arbitrary assumptions, namely,

i) that the additive intake drag is not considered to be a major influence on net thrust characteristics, and

ii) that the intake flow transforms the scooped-up portion of the boundary layer into a one-dimensional flow within a constant cross-section passage.

In view of these arbitrary assumptions, experimental data on intakes must be utilized to contribute to a better judgement on the merits of the theory. In particular, experimental information can be applied to improve on assumption ii), above, by introducing an efficiency for total pressure recovery such that

$$\eta = (P_{os}/P_{o\infty})\ \text{Actual} \Big/ (P_{os}/P_{o\infty})\ \text{Theoretical}^{7}$$

As reliable information on such intake efficiencies becomes available, the attractiveness of the theoretical analysis is enhanced. The narrow limits for η which have been established experimentally for well-designed intakes thus will give weight to the theoretical analysis of intake performance.

3.2.1 Theoretical Intake Analysis

According to the assumptions advanced by Simon and Kowalski[7], one may analyze intake performance on the basis of knowing the approaching flow conditions in the free stream (P_∞, M_∞) and in the boundary layer just ahead of the intake (δ, n). By direct application of this analysis, and by considering the flow in the boundary layer at the afterbody radius R_o as essentially two-dimensional, one utilizes the following relations:

$$(m/m_\ell) = f(n,\ M_\infty,\ r/\delta) \qquad (5)$$

and

$$(P_{os}/P_{o\infty})\ \text{Theo.}^{7} = \frac{(P_\infty/P_{o\infty})_{M_\infty}}{(P_s/P_{os})_{M_s}} \cdot \frac{m}{m_\ell} \cdot \frac{(\frac{A}{A^*}\frac{P}{P_o})_{M_s}}{(\frac{A}{A^*}\frac{P}{P_o})_{M_\infty}} \tag{6}$$

where M_s can be determined from

$$(F/F^*)_{M_s} = \frac{\frac{\Phi}{\Phi_\ell}(n,\ M_\infty,\ \frac{r}{\delta})}{\frac{m}{m_\ell}(n,\ M_\infty,\ \frac{r}{\delta})} \cdot (\frac{F}{F^*})_{M_\infty} \tag{7}$$

Utilizing the graphical presentations[7], relationships of the following functional form can be determined.

$$(\frac{m}{m_\ell} \cdot \frac{r}{\delta}) = f(n,\ M_\infty,\ \frac{r}{\delta}) \tag{8}$$

and

$$(\frac{P_{os}}{P_{o\infty}}) = f(n,\ M_\infty,\ \frac{r}{\delta}) \tag{9}$$

The momentum of the intake air will be related to

$$(\frac{r}{\delta} \cdot \frac{\varphi}{\varphi_\ell}) = f(n,\ M_\infty,\ \frac{r}{\delta})$$

While these relations do not depend on any specific information concerning the intake geometry (except for the assumption of constant area mixing), a given intake geometry will introduce a possible choking cross section, A_C, and for a given flight condition, establish the efficiency η. Both of these factors contribute to the choking limit of an actual intake which is of special interest in the matching problem.

3.2.2 Utilization of Experimental Intake Data

Experimental intake data are usually given in the form[8]

$$\frac{P_{os}}{P_{o\infty}} = f\ (\text{geometry},\ \frac{\delta}{L_{ref}},\ n,\ M_\infty,\ \frac{m_s}{m_o})$$

where

$$\frac{m_s}{m_o} = \frac{m_s}{A_o P_\infty V_\infty} \quad \text{and } M_\infty$$

are the controlled test variables for a given inlet geometry, while $\frac{\delta}{L_{ref}}$ and n are usually not subject to systematic variations. The latter represents a definite shortcoming for any wider interpretation of experimental results, especially in view of the large influence of boundary layer thickness. The theoretical analysis which covers the latter influence can therefore be used with advantage, provided sufficient confidence can be established for η values determined with the help of experimental investigations.

To compare theoretical and experimental intake data, note that for two-dimensional intakes,

$$\left(\frac{m_s}{m_\ell} \cdot \frac{r}{\delta}\right) = \frac{m_s}{m_o} \cdot \frac{A_o}{\delta} \qquad (10)$$

where A_o is the area per unit width of the intake.

In any case, the efficiency η may be considered as a parameter in the theoretical calculations which will show (see section 5.2) the importance of designing efficient intakes and also indicate the levels required to achieve satisfactory thrust levels for air-augmented systems.

Intake drag data can be obtained from either measured static pressure distributions and estimated shear forces or from direct force balance measurements. In addition, choking limits for given intakes (within the limitations of possibly uncontrolled boundary layer thickness effects) are obviously obtained in the experiments.

4. MATCHING OF EJECTOR AND INTAKE OPERATING CONDITIONS

In principle, the matching procedure is illustrated by the intersection of the ejector surface with the intake surface, see Figure 7. It must, however, be remembered that the ejector surface appears in the $\frac{W_s}{W_p} = f\left(\frac{P_\infty}{P_{op}}, \frac{P_{os}}{P_{op}}\right)$ diagram while the intake surface is originally defined functionally by the relations

$$\frac{m}{m_\ell} = f\left(\frac{P_{os}}{P_{o\infty}}\right) \quad \text{or} \quad \frac{m}{m_o} = f\left(\frac{P_{os}}{P_{o\infty}}\right)$$

A transformation into a common coordinate system must be made[9].

The internal ejector performance now has to be interpreted in terms of external flow parameters while the intake performance has to be interpreted for a specific internal and external afterbody geometry.

Depending on whether theoretical or experimental intake data are to be utilized, the matching procedure will assume different forms.

4.1 Matching of Ejector and Intake (Theoretical Intake Analysis)

The application of the continuity equation for a given geometry R_{1p}/R_o, a convergent primary nozzle, and external flow conditions M_∞ and δ/R_o yields the following relationship which is used in the matching procedure. For $K_p = K_s = K$,

$$\left(\frac{m}{m_\ell}\cdot\frac{r}{\delta}\right)_{n,\ M_\infty,\ \frac{r}{\delta}} = \left\{\frac{P_{op}}{P_{os}}\right\}\cdot\left\{\frac{1}{2}\left(\frac{2}{K+1}\right)^{\frac{K+1}{2(K-1)}}\right\}\cdot\left\{\frac{R_{1p}}{R_o}\right\}^2\cdot\left\{\frac{R_o}{\delta}\right\}\cdot\left\{\frac{W_s}{W_p}\right\}\cdot$$

$$\left\{\frac{1}{M_\infty}\cdot\frac{\sqrt{(T/T_o)}}{(P/P_o)}\right\}_{M_\infty}\cdot\left\{\frac{P_{os}}{P_{o\infty}}\right\} \qquad (11)$$

The matching is achieved as follows:

For a selected operating point of the ejector, see Figure 5, one obtains the product

$$\left\{\frac{P_{op}}{P_{os}}\ \frac{W_s}{W_p}\right\}$$

The ejector geometry determines R_{1p}/R_o and primary nozzle geometry, here convergent, is implicitly contained in the above pressure ratio-mass flow rate product. The flight conditions contribute information on M_∞, n, and δ/R_o. The left side of the equation can now be expressed as a function of $\frac{r}{\delta}$, with n and M_∞ being fixed.

The only remaining term on the right side of the equation is $\frac{P_{os}}{P_{o\infty}}$, which according to Simon and Kowalski, can be theoretically evaluated as $\frac{P_{os}}{P_{o\infty}} = f(n,\ M_\infty,\ \frac{r}{\delta})$. Hence, $\frac{r}{\delta}$ can be considered as a trial variable for calculating and matching both sides of equation (11), hence obtaining the operating condition, that is, the correct value for $\frac{r}{\delta}$, and $\frac{m}{m_\ell}(n,\ M_\infty,\ \frac{r}{\delta})$, and subsequently, $\frac{P_{os}}{P_{o\infty}}(n,\ M_\infty,\ \frac{r}{\delta})$.

To improve the quantitative aspects of the intake analysis, the intake efficiency, η, which has been defined in section 3.2, can be introduced as a parameter. This matching procedure is illustrated graphically in Figure 9.

It should be noted that aside from the use of an intake efficiency, the actual shape of the intake has not been considered. Intake design must, however, be concerned with determining the choking limit, which will depend upon a minimum cross section in the intake passage. A discussion of intake operating conditions (subcritical, critical, or supercritical) will be given in the following section.

4.2 Matching Experimental Intake Data

Experimental data defining the internal performance of an inlet are generally presented in the form[8]

$$\frac{P_{os}}{P_{o\infty}} = f\left(\frac{\delta}{L_{ref}},\ M_\infty,\ \frac{m_s}{m_o}\right) \tag{12}$$

where

$$\frac{m_s}{m_o} = \frac{m_s}{\rho_\infty V_\infty A_o}$$

A_o being a reference inlet area.

In analogy to the procedure developed in section 4.1, we may now establish

$$\frac{m_s}{m_o} = \underbrace{\left\{\frac{P_{op}}{P_{os}} \cdot \frac{W_s}{W_p}\right\}}_{\text{Ejector}} \cdot \underbrace{\left\{\sqrt{\frac{T_{op}}{T_p^*}} \cdot \frac{P^*}{P_{op}}\right\}}_{\text{Primary Nozzle}} \cdot \underbrace{\left\{\frac{R_1 p^2 \pi}{A_o}\right\}}_{\text{Geometry}} \cdot \underbrace{\left\{\frac{1}{M_\infty} \cdot \sqrt{\frac{T_\infty}{T_{o\infty}}} \cdot \frac{P_{o\infty}}{P_\infty}\right\}_{M_\infty}}_{\text{Free-stream}} \cdot \underbrace{\frac{P_{os}}{P_{o\infty}}}_{\text{Intake}}$$

and obtain the match point by simultaneously satisfying Equation 12.

As an alternative, the well-known matching procedure of Reference 9 can also be utilized by establishing "converted" inlet and ejector maps.

The latter method is of special interest since it also locates the match point relative to the choking limit of the intake. A conventional inlet map of the form

$$\frac{P_{os}}{P_{o\infty}} = f\left(\frac{m_s}{m_o},\ M_\infty,\ \frac{\delta}{L_{ref}}\right)$$

is converted into a

$$\frac{P_{os}}{P_{o\infty}} = f\left(\frac{W_s}{W_p},\ M_\infty,\ \frac{\delta}{L_{ref}}\right)$$

plot by transforming, for the given free stream Mach number M_∞, the abscissa

$$\frac{W_s}{W_p} = \left(\frac{m_s}{m_o}\right) \cdot \left(\frac{A_o}{\pi R_{1p}^2}\right) \cdot \left(\frac{P_{op}}{P^*}\right) \cdot \left\{ M_\infty \sqrt{\frac{T_{o\infty}}{T_\infty}} \cdot \frac{P_\infty}{P_{op}} \right\}_{M_\infty} \tag{13}$$

where $\frac{P_\infty}{P_{op}}$ remains a parameter. The conventional ejector map $\frac{P_{os}}{P_{op}} = f\left(\frac{W_s}{W_p}\right)$ is converted by transforming, for a given free stream Mach number M_∞, the ordinate so that

$$\frac{P_{os}}{P_{o\infty}} = \left\{\frac{P_{os}}{P_{op}}\right\} \cdot \left\{\frac{P_{op}}{P_\infty}\right\} \cdot \left\{\frac{P_\infty}{P_{o\infty}}\right\}_{M_\infty} \tag{14}$$

the primary nozzle pressure ratio will again serve as a parameter. Any given flight schedule will specify the relation between $\frac{P_{op}}{P_\infty}$ and M_∞, so that selection of M_∞ will determine the parametric value of $\frac{P_{op}}{P_\infty}$. The performance curves of the ejector and the intake having this same primary nozzle pressure ratio will then intersect at the "match point."

The location of the match point relative to the choking portion of the inlet performance curve is immediately recognized for experimentally determined intake characters. However, converted intake and ejector charts can also contribute to the understanding of operating conditions of "theoretical" intakes, for which choking will occur when

$$\left\{\frac{W_s}{W_p}\right\}_C = \left(\frac{2}{K_s+1}\right)^{\frac{K_s+1}{2(K_s-1)}} \cdot \left\{\frac{P_{o\infty}}{P_\infty}\right\}_{M_\infty} \cdot \left\{\frac{A_o}{R_{1p}^2 \pi}\right\} \cdot \left\{\frac{K_p+1}{2}\right\}^{\frac{K_p}{K_p-1}} \cdot \eta \cdot \frac{P_{os}}{P_{o\infty}} \cdot \frac{P_\infty}{P_{op}} \tag{15}$$

4.3 Net Afterbody Thrust Evaluation

The matching procedure of section 4.1, carried out for a given point of the internal ejector characteristic $\left(\frac{P_{os}}{P_{op}}, \frac{W_s}{W_p}\right)$, and a selected flight condition $\left(M_\infty, \frac{\delta}{R_o}, n\right)$, determined the intake operating condition and hence, $\frac{P_{os}}{P_{o\infty}}$, so that the primary nozzle pressure ratio is found from equation (14)

$$\frac{P_{op}}{P_\infty} = \frac{P_{op}}{P_{os}} \cdot \frac{P_{os}}{P_{o\infty}} \cdot \frac{P_{o\infty}}{P_\infty} \tag{16}$$

4.3.1 Gross Thrust

The gross thrust can now be determined according to equation (1), which is here repeated for convenience,

$$\bar{F}_{Gross} = \int_{E_{CP}} (P-P_\infty)\, d\bar{S}_E + \int_{E_{CP}} \rho\, \bar{V}(\bar{V}\cdot d\bar{S}_E) + \int_{E_{CS}} (P-P_\infty)\, d\bar{S}_E + \int_{E_{CS}} \rho\, \bar{V}(\bar{V}\cdot d\bar{S}_E) + \int_{E_{SH}} (P-P_\infty)\, d\bar{S}_E \qquad (1)$$

as follows:

i) by determining the thrust contribution of the primary nozzle

$$F_{1D,C} = \int_{E_{CP}} (P-P_\infty)\, d\bar{S}_E + \int_{E_{CP}} \rho\, \bar{V}(\bar{V}\cdot d\bar{S}_E)$$

ii) by evaluating the integrals relating to the secondary flow

$$\int_{E_{CS}} (P-P_\infty)\, d\bar{S}_E + \int_{E_{CS}} \rho\, \bar{V}(\bar{V}\cdot d\bar{S}_E)$$

from the ejector code, including the viscous correction for the pumping characteristic, and

iii) by considering the thrust contribution of the internal shroud surface

$$\bar{F}_{SH} = \int_{E_{SH}} (P-P_\infty)\, d\bar{S}_E,$$

which will include the contribution of the hydrostatic pressures, obtained from the inviscid ejector code calculation, $\int_{E_{SH}} (P-P_\infty)\, d\bar{S}_E$/hydrostatic, and the effect of wall friction ($-\Delta F_{B.L.}$). The latter is found with the help of a boundary layer program (see section 3.1.3). Of particular interest is the momentum thickness at the exit cross section of the ejector which determines the loss of gross thrust due to shroud wall friction; this loss is given by:

$$\Delta F_{B.L.} = \pi R_{1p}^2\, P_{op} \left(\frac{P_{os}}{P_{op}}\right)\left(\frac{R_o}{R_{1p}}\right)\left(K_s M_e^2 \frac{P_e}{P_{os}}\right)\, 2\frac{\theta}{R_{1p}}(H+1) \qquad (17)$$

4.3.2 Intake Thrust Force

Since the present paper is primarily concerned with the theoretical evaluation of air-augmented systems, the results of sections 3.2.1 and 4.1 will be of principal

interest. For matched conditions, the intake momentum charge (for nearly two-dimensional flow) is found from

$$\int_{I_{C1}} \rho \bar{V} (\bar{V} \cdot d\bar{S}_I) = 2\pi R_o \int_o^r \rho V^2 \, dy = 2\pi \delta^2 \frac{R_o}{\delta} \cdot \frac{P_\infty}{P_{o\infty}} \cdot P_{o\infty} M_\infty^2 \left(\frac{\varphi}{\varphi_\ell} \cdot \frac{r}{\delta}\right)$$

where

$\left(\frac{\varphi}{\varphi_\ell} \cdot \frac{r}{\delta}\right) = f\left(M_\infty, n, \frac{r}{\delta}\right)$ is presented graphically in reference 7.

4.3.3 Net Afterbody Thrust Force

It was pointed out before that both the additive intake drag and the boattail drag would not be considered explicitly. Therefore, we restrict ourselves to the evaluation of

$$\left(\bar{F}_{net} - \bar{F}_B + \bar{F}_{l_A}\right) = \bar{F}_{Gross} - \int_{I_{C1}} (P - P_\infty) \, d\bar{S}_I - \int_{I_{C1}} \rho \bar{V} (\bar{V} \cdot d\bar{S}_I)$$

4.3.4 Reference Thrust Forces

For the purpose of easier discussion of the results obtained for specific air-augmented systems, the ideal thrust forces of certain specified non-augmented primary nozzles are introduced as reference values.

4.3.4.1 Using as a reference the ideal convergent nozzle having a thrust force of

$$F_{ID,C} = A^* P^* \left[(1+K_P) - \frac{P_\infty}{P_{op}} \cdot \left(\frac{K_p + 1}{2}\right)\right]^{\frac{K_p}{K_p - 1}}$$

4.3.4.2 Using as a reference the ideal, fully adjustable, convergent-divergent nozzle, having a thrust force of

$$F_{ID} = K_P P_\infty A_e M_e^2 = A^* P^* \left[K_P \left(\frac{K_P + 1}{2}\right)^{\frac{K_P}{K_P - 1}} \cdot \frac{P_\infty}{P_{op}} \frac{A_e}{A^*} M_e^2\right]$$

5. IN-FLIGHT PERFORMANCE EVALUATION OF AN AIR-AUGMENTED JET ENGINE NOZZLE

Shown in figure 8 is a schematic sketch of the system to which the foregoing

analysis has been applied. The same configuration has been evaluated, in static tests only, by Huntley and Yanowitz, reference 10**. Specifically for this configuration, $\frac{R_o}{R_{1p}} = 1.31$, $\frac{L}{R_{1p}} = 1.75$, and a conical divergence angle of the shroud of 3.82°. To evaluate the friction effects on the internal shroud wall, a value of Reynolds Number, $\frac{a_{os}}{\nu_{os}} R_{1p} = 10^5$, was used for the experimental conditions reported. (The effects of internal wall friction were found to be small for the cases investigated; the maximum value found was less than 0.3% of the gross thrust.)

In addition, it was assumed for the in-flight performance analysis that $\frac{\delta}{R_o} = 0.2$ and $\frac{a_{o\infty}}{\nu_{o\infty}} R_o = 10^5$ for all conditions.

The results of the theoretical gross thrust calculations, as compared to experimental data reported in reference 10 has already been shown in figure 6. In addition, the comparison is presented in a different form in figure 8-B.

5.1 Flight Schedule

Selection of a single internal ejector performance point results in a fixed flight schedule, as shown in figure 10. However, the theoretical analysis could match any given or desired flight schedule by repeating the calculations for other operating points of the internal ejector characteristic (figure 5).

5.2 Comparison With an Ideal Converging Nozzle

Theoretical in-flight characteristics for the chosen internal operating point, as affected by parametric values of intake efficiencies (see section 3.2, ii) are shown in figure 11, using as a reference the convergent nozzle. The selected example immediately reveals the importance of high intake efficiencies. Even then, for obtainable values of intake efficiencies, the direct improvement remains marginal. One should, however,

** The configuration investigated by Huntley and Yanowitz is attractive for the present analysis because it incorporates a relatively long and non-cylindrical ejector shroud in contrast to other geometries for which in-flight performance data has been reported[11, 12].

keep in mind that the installed performance of the convergent nozzle could suffer substantially from the high transonic base pressure drag penalties due to jet-slip-stream interaction -- a situation which could largely be avoided by the present air-augmented configuration.

5.3 Comparison With an Ideal Fully Expanded C-D Nozzle

When using the ideal fully adjustable C-D nozzle as reference, the selected air-augmented system immediately fails to qualify as a thrust-augmentation scheme, at least when the reference nozzle is not penalized for slip-stream interaction or for differences in boattail drag, see figure 12.

6. CONCLUSIONS

The presented method of theoretical analysis allows an evaluation of static and in-flight performance for air-augmented systems. While the present analysis remained restricted to cold primary streams, an extension to hot operation including reactive mixing[13] is possible.

Comparison between calculated and experimental gross thrust performance was possible and indicated good agreement, with the theoretical analysis giving slightly conservative results which can be attributed to the simplified treatment of the intake flow.

The selection of a specific configuration, namely an air-augmented jet engine designed for operation through the transonic flight regime, was consistent with the present status of ejector computer codes at the University of Illinois which allow consideration of non-cylindrical ejector shrouds but are momentarily limited to only moderately underexpanded or overexpanded primary jets. The restriction to a convergent primary nozzle was not essential for the general procedure.

Future studies can be carried out with the help of revised ejector codes which will allow the theoretical evaluation of air-augmented rocket systems involving convergent-

divergent primary nozzles, larger primary nozzle pressure ratios, larger shroud to nozzle diameter ratios, and hot or even reacting primary jets.

REFERENCES

1) Air Augmentation: A Role in Missile and Launch Vehicle Growth Programs, by Thomas E. Dolan, Minutes of the 31st Meeting, May 19-20, 1964. Vol. 1, pp. 137-160. Bumblebee Propulsion Panel, Applied Physics Laboratory - Howard County, Maryland. (Conf.)

2) Investigation of Vehicle-Integrated Rocket Powerplants With Air Augmentation, Vol. 1 and 2, Final Report.
Prepared for the National Aeronautics and Space Administration, George C. Marshall, Space Flight Center, Huntsville, Alabama, under Contract NAS 8-11017, by the Boeing Company, June 15, 1964. (Conf.)

3) "Interaction Between Primary and Secondary Streams of Supersonic Ejector Systems and Their Performance Characteristics," by W. L. Chow and A. L. Addy. AIAA Journal, Vol. 2, No. 4, pp. 686-695, 1964.

4) "Characteristics of Supersonic Ejector Systems with Nonconstant Area Shroud," by W. L. Chow and P. S. Yeh, AIAA Journal, Vol. 3, No. 3, pp. 526-527.

5) "Drag of Conical and Circular-Arc Boattail Afterbodies at Mach Numbers From 0.6 to 1.3," by Frank V. Silhan and James M. Cubbage, Jr., NACA RM L56 K22, January 1957.

6) "Jet Effects on the Drag of Conical Afterbodies for Mach Numbers of 0.6 to 1.28," by James M. Cubbage, Jr., NACA RM L57 B21, April 1957.

7) "Charts of Boundary-Layer Mass Flow and Momentum for Inlet Performance Analysis Mach Range, 0.2 to 5.0," by Paul C. Simon and Kenneth L. Kowalski, NACA TN 3583, November 1955.

8) "A Transonic Investigation of the Mass-Flow and Pressure Recovery Characteristics of Several Types of Auxiliary Air Inlets," by John S. Dennard, NACA RM L57 B07, April 1957.

9) "Matching of Auxiliary Inlets to Secondary-Air Requirements of Aircraft Ejector Exhaust Nozzles," by Donald P. Hearth, Gerald W. Englert, and Kenneth L. Kowalski, NACA RM E55 D21, August 1955.

10) "Pumping and Thrust Characteristics of Several Divergent Cooling-Air Ejectors and Comparison of Performance With Conical and Cylindrical Ejectors," by S. C. Huntley and Herbert Yanowitz, NACA RM E53 J13, January 1954.

11) "Thrust and Pumping Characteristics of a Series of Ejector-Type Exhaust Nozzles at Subsonic and Supersonic Flight Speeds," by Donald P. Hearth and Alfred S. Valerino, NACA RM E54 H19, November 1954.

12) "Effect of Free-Stream Mach Number on Gross-Force and Pump Characteristics of Several Ejectors," by Leonard E. Stett and Alfred S. Valerino, NACA RM E54 K23a, March 1955.

13) "The Effect of Chemical Reactions in the Turbulent Mixing Component on the Dynamics and Thermodynamics of Wake Flow Fields," by L. R. Davis, Ph.D. thesis, Department of Mechanical Engineering, University of Illinois, June 1964.

NOMENCLATURE

a	Velocity of sound
A	Area when subscripted
A, B, C	Coefficients in equation defining the shroud wall contour
D	Diameter
E	Areas in ejector control domain
F	Force or thrust
f	Functional relationship
H	Boundary layer form factor
I	Areas in Intake control domain
K	Ratio of specific heats
L	Ejector shroud length
M	Mach number
m	Mass flow rate (intake)
n	Boundary layer velocity profile exponent
P	Pressure
R	Radius, radial coordinate or gas constant
r	Normal distance from boundary layer generating surface to intake lip
S	Area in control domain analysis
T	Absolute temperature
V	Velocity

W Mass flow rate (ejector)

Z Longitudinal coordinate

$(\frac{m}{m_\ell} \cdot \frac{r}{\delta})$ Product of the mass-flow-rate ratio and the intake height-to-boundary layer thickness for the theoretical intake analysis, reference 7.

$(\frac{m}{m_o} \cdot \frac{r}{\delta})$ Product of the mass-flow-rate ratio and the intake height-to-boundary layer thickness for the experimental intake analysis, reference 8.

$(\frac{P_{os}}{P_{o\infty}})_{\text{Theoretical}^7}$ Intake recovery pressure ratio, reference 7.

δ Boundary layer thickness

η Intake pressure recovery efficiency referenced to the theoretical values of reference 7.

θ Streamline angle or boundary layer momentum thickness

ν Kinematic viscosity

ρ Radius of curvature or density

$\frac{\Phi}{\Phi_\ell}(n, M_\infty, \frac{r}{\delta})$ Defined in reference 7

$(\frac{r}{\delta} \cdot \frac{\varphi}{\varphi_\ell})$ Defined in reference 7

Subscripts

o Stagnation conditions

1 Section 1

2 Section 2

∞ Free-stream

A Additive

Act. Actual conditions

B Boattail

B.L. Boundary layer

C Where mass is "crossing" or "choking"

E Ejector

G "Gross"

I	Intake
ID	Ideal fully expanded nozzle
ID, C	Ideal Converging nozzle
M_s	Function of M_s
M_∞	Function of M_∞
n	Function of n
Net	Net value
OB	Obstruction
P	Primary Stream
$\frac{r}{\delta}$	Function of $\frac{r}{\delta}$
Ref	Reference value
S	Secondary stream
SH	Shroud
W	Shroud wall

Superscripts

*	Sonic conditions

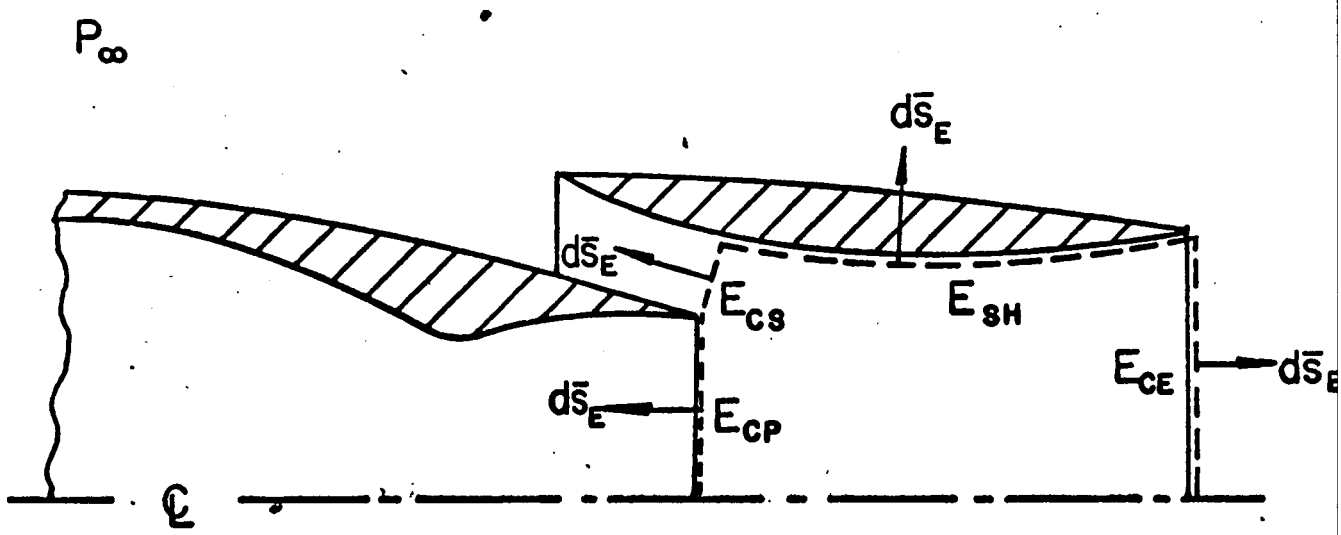

$$\bar{F}_{GROSS} = -\int_{E_{CE}} (P - P_\infty)\, d\bar{s}_E - \int_{E_{CE}} \rho \bar{V} (\bar{V} \cdot d\bar{s}_E)$$

$$= \bar{F}_{SH} + \int_{E_{CP}} (P - P_\infty)\, d\bar{s}_E + \int_{E_{CP}} \rho \bar{V} (\bar{V} \cdot d\bar{s}_E) +$$

$$\int_{E_{CS}} (P - P_\infty)\, d\bar{s}_E + \int_{E_{CS}} \rho \bar{V} (\bar{V} \cdot d\bar{s}_E)$$

FIG. 1 CONTROL DOMAIN FOR EJECTOR ANALYSIS (GROSS THRUST FORCE)

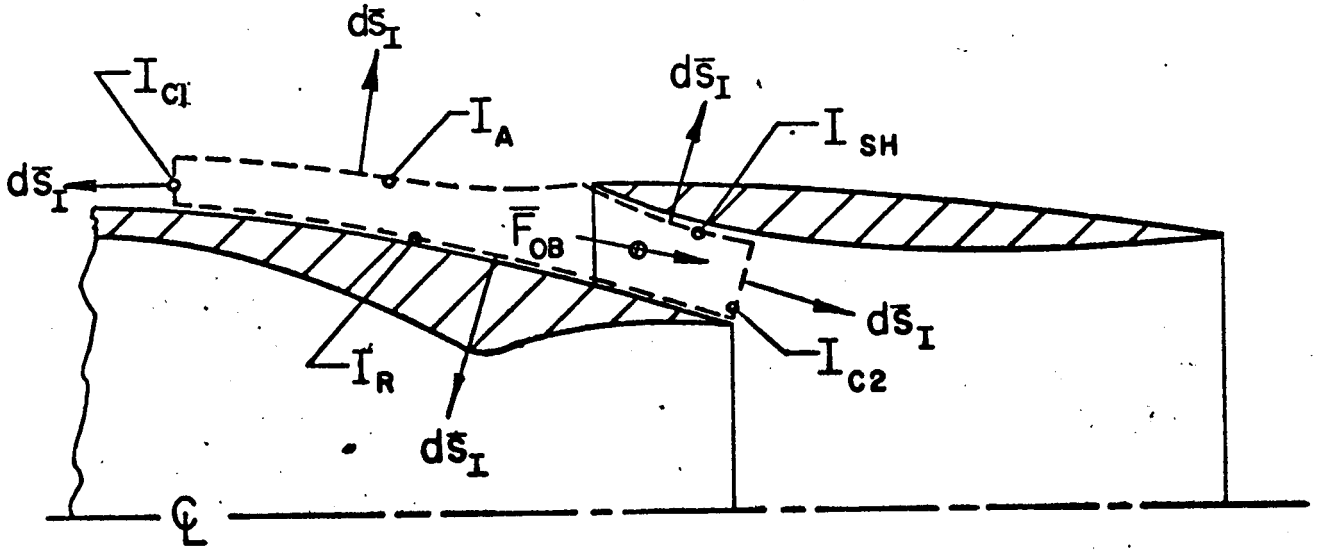

$$\bar{F}_{I_A} + \bar{F}_{I_R} + \bar{F}_{I_{SH}} + \bar{F}_{I_{OB}} = -\int_{I_{C1}} (\bar{P} - \bar{P}_\infty)\, d\bar{S}_I - \int_{I_{C1}} \rho \bar{V} (\bar{V} \cdot d\bar{S}_I)$$
$$-\int_{I_{C2}} (P - P_\infty)\, d\bar{S}_I - \int_{I_{C2}} \rho \bar{V} (\bar{V} \cdot d\bar{S}_I)$$

FIG. 2 CONTROL DOMAIN FOR INTAKE ANALYSIS

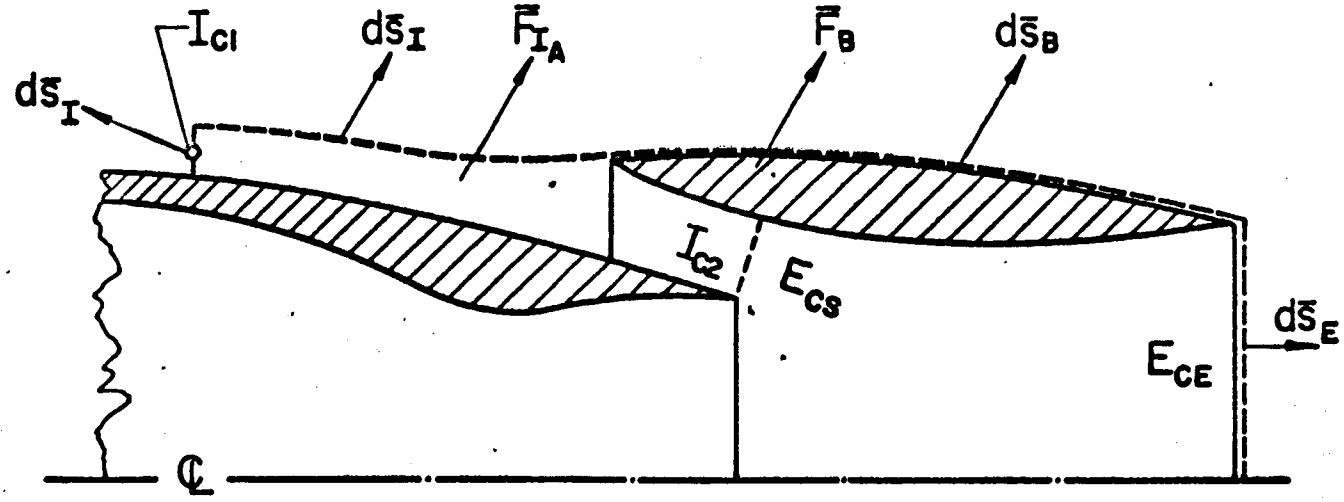

$$\bar{F}_{NET} = \bar{F}_{GROSS} - \bar{F}_{I_A} + \bar{F}_B - \int_{I_{C1}} (P - P_\infty) d\bar{s}_I - \int_{I_{C1}} \rho \bar{V} (\bar{V} \cdot d\bar{s}_I)$$

WHERE:

$$\bar{F}_{I_A} \text{ (ADDITIVE DRAG)} = - \int_{I_A} (P - P_\infty) d\bar{s}_I$$

$$\bar{F}_B \text{ (BOATTAIL DRAG)} = - \int_B (P - P_\infty) d\bar{s}_B$$

$\bar{F}_{NET}$ CAN ALSO BE REPRESENTED BY:

$$\bar{F}_{NET} = \sum \bar{F}_{SHROUD} + \bar{F}_{I_R} + \bar{F}_{I_{OB}} + \int_{E_{CP}} (P - P_\infty) d\bar{s}_E + \int_{E_{CP}} \rho V (V \cdot d\bar{s}_E)$$

WHERE:

$$\sum \bar{F}_{SHROUD} = \bar{F}_{E_{SH}} + \bar{F}_{I_{SH}} + \bar{F}_B$$

FIG. 3 CONTROL DOMAIN FOR ANALYSIS OF NET AFTERBODY THRUST FORCE.

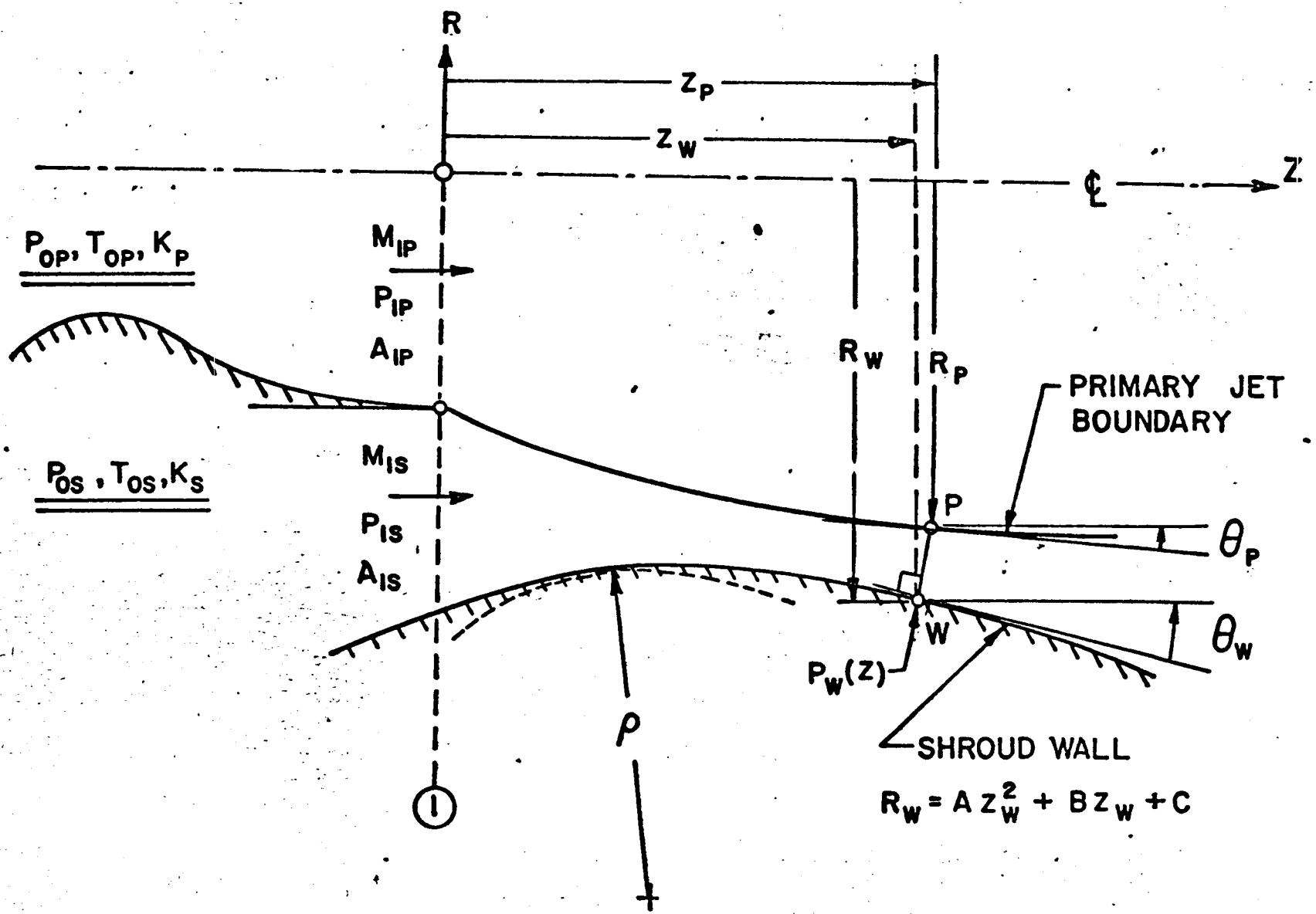

FIG. 4 EJECTOR CONFIGURATION AND NOTATION.

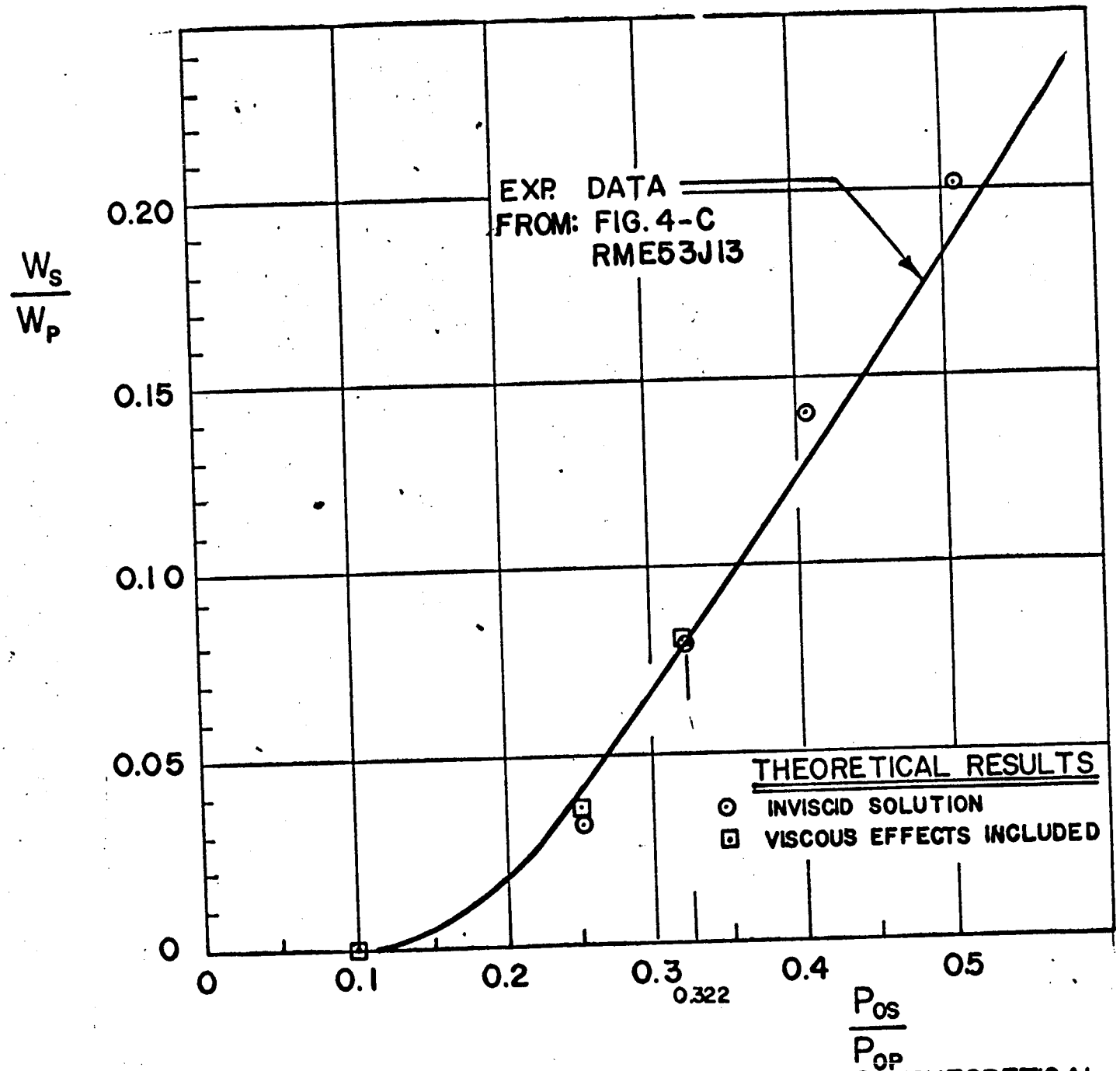

FIG. 5 COMPARISON OF EXPERIMENTAL & THEORETICAL EJECTOR PUMPING CHARACTERISTICS

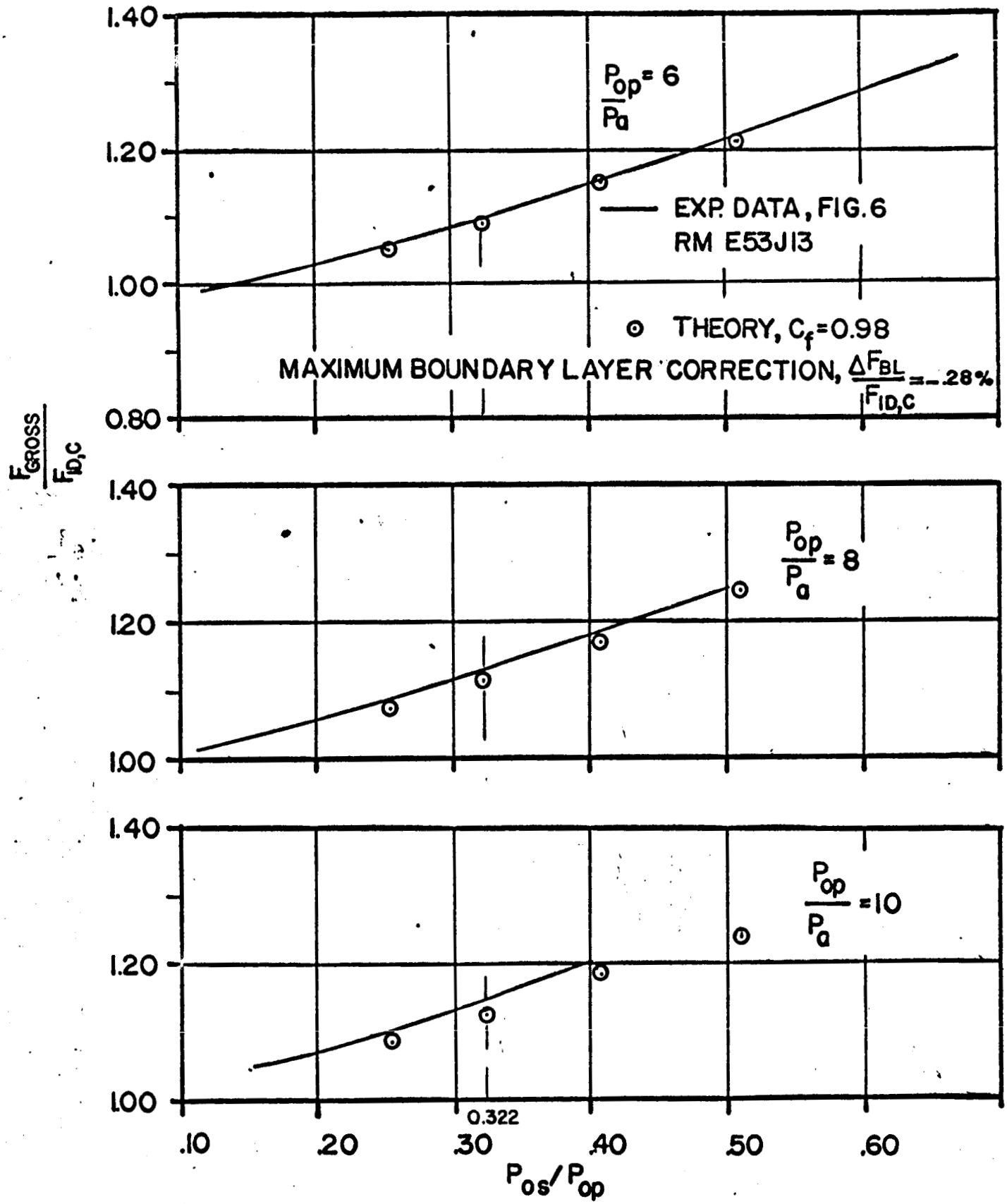

FIG. 6 COMPARISON OF THRUST CHARACTERISTICS FOR STATIC OPERATION OF A DIVERGENT EJECTOR

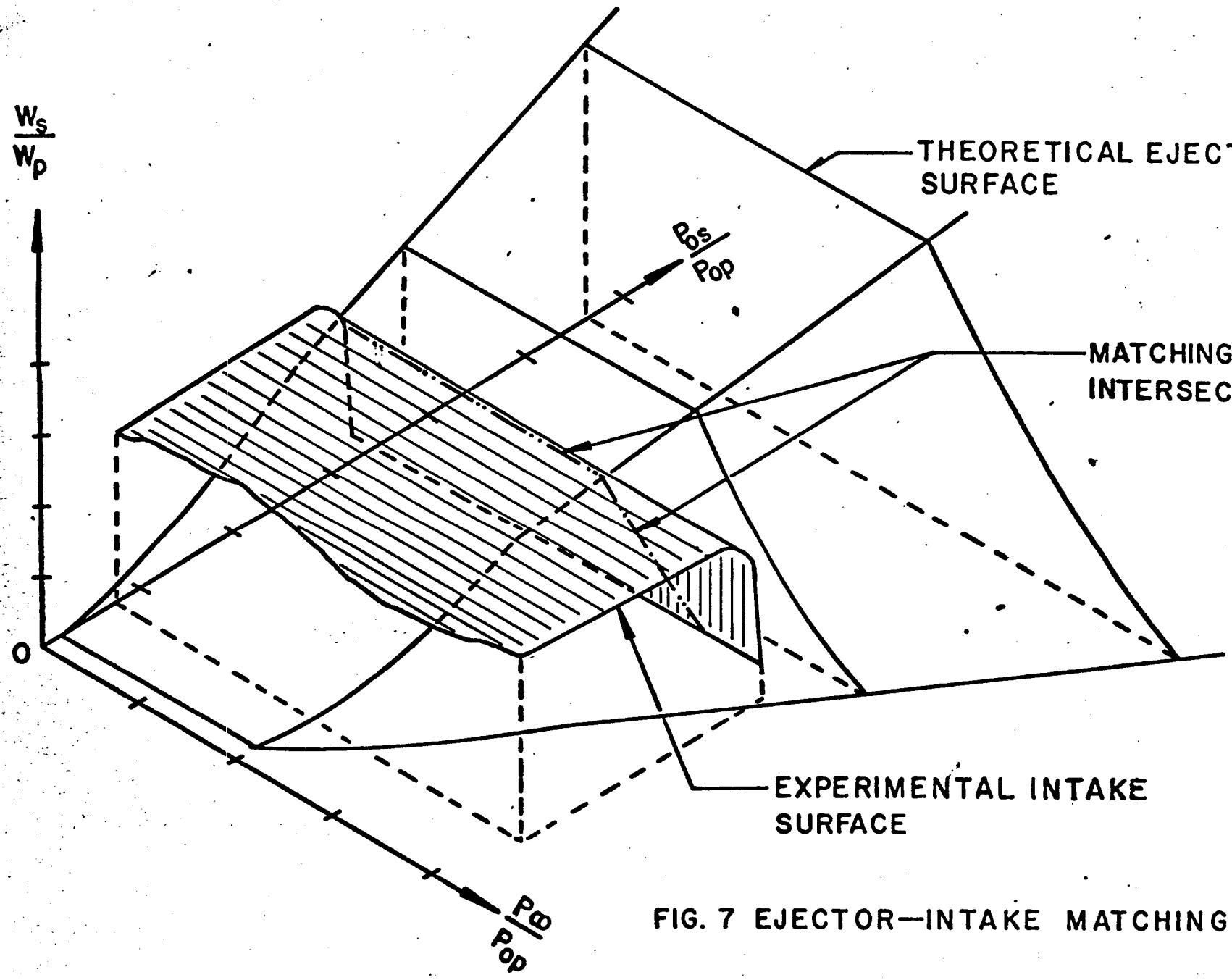

FIG. 7 EJECTOR—INTAKE MATCHING

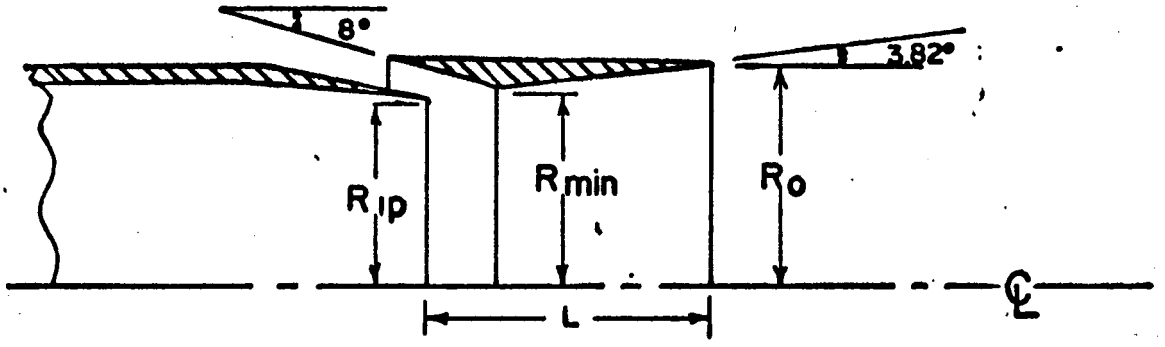

$R_{MIN}/R_{IP} = 1.21$, $R_o/R_{IP} = 1.31$

$L/2R_{IP} = 0.874$

FIG. 8-A NACA CONFIGURATION FOR STATIC THRUST EXPERIMENTS (RM E 53J13)

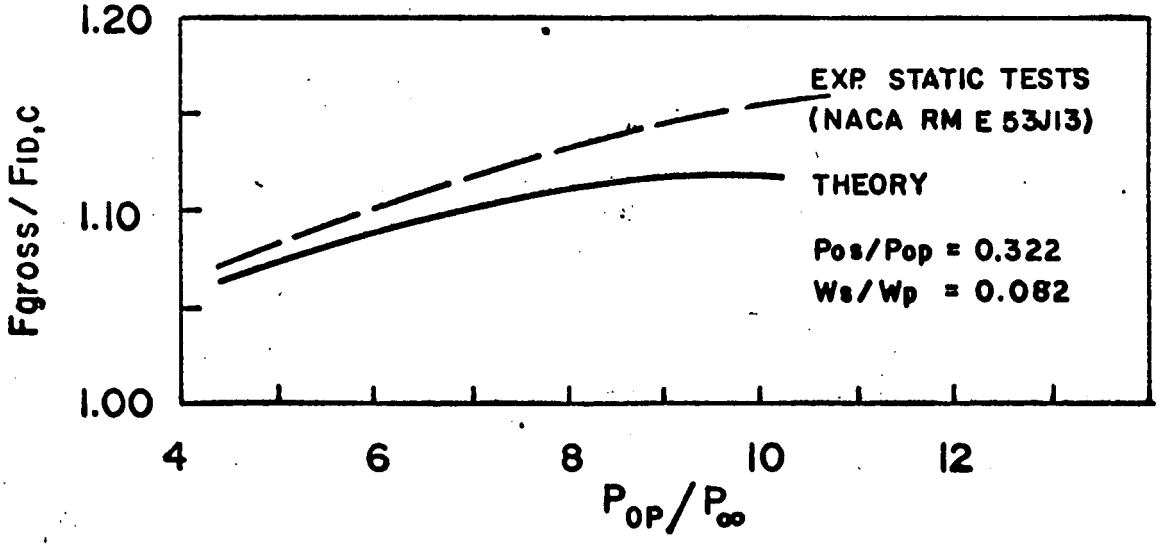

FIG. 8-B COMPARISON OF THEORETICAL AND EXPERIMENTAL STATIC THRUST CHARACTERISTICS FOR ONE EJECTOR OPERATING POINT

LEGEND: I - INTAKE (NACA TN 3583)
E - EJECTOR (THEORETICAL)
Δ - MATCH POINTS

DATA: $\delta / R_0 = 0.2$, $R_0 / R_{IP} = 1.31$

$P_{OS} / P_{OP} = 0.322$, $W_S / W_P = 0.082$

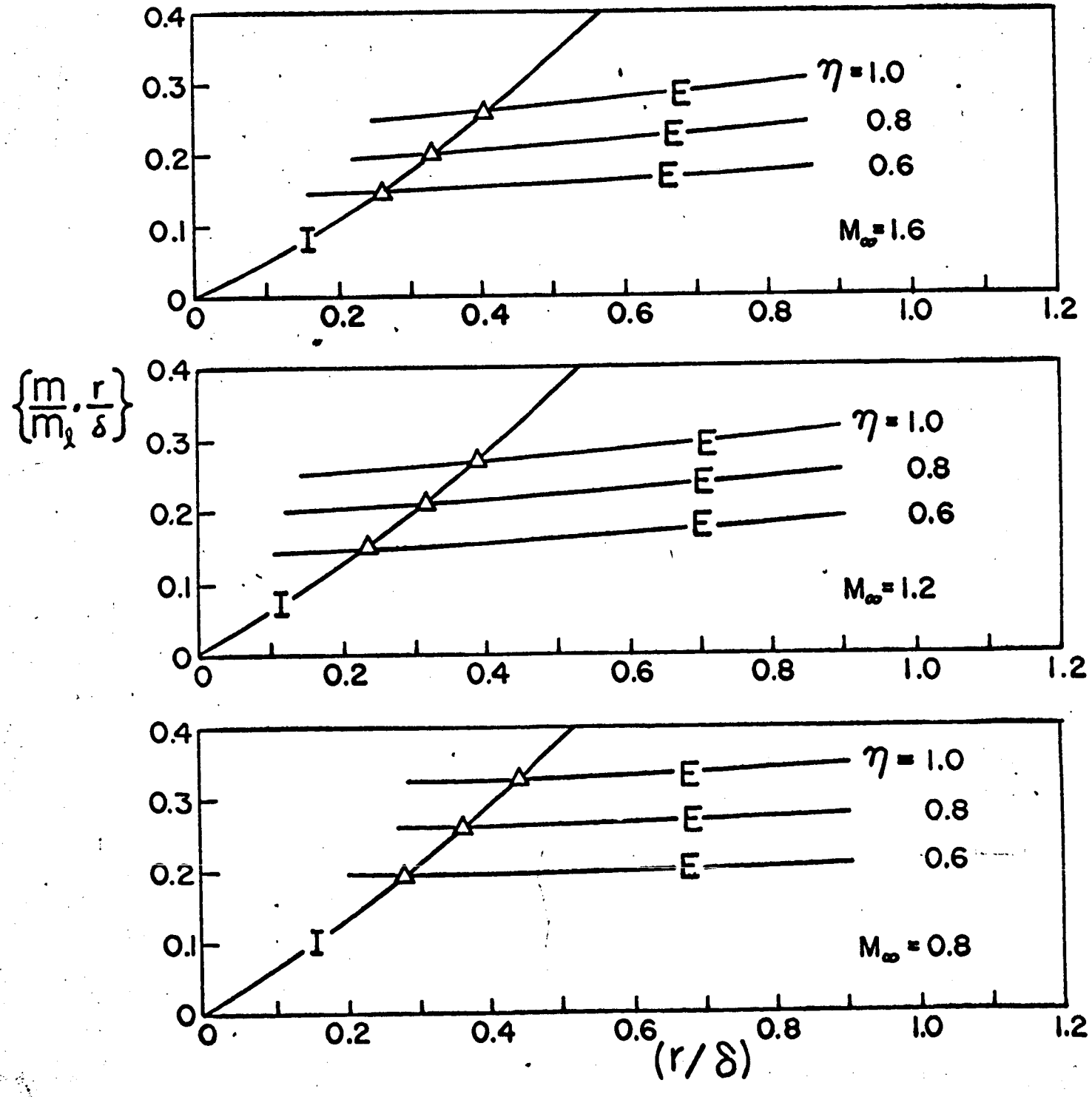

FIG. 9 THEORETICAL MATCHING OF INTAKE AND EJECTOR

DATA: $\delta / R_0 = 0.2$, $R_0 / R_{ip} = 1.31$

$P_{0s} / P_{0P} = 0.322$, $W_s / W_p = 0.082$

CONFIGURATION: SEE FIG. 8-A

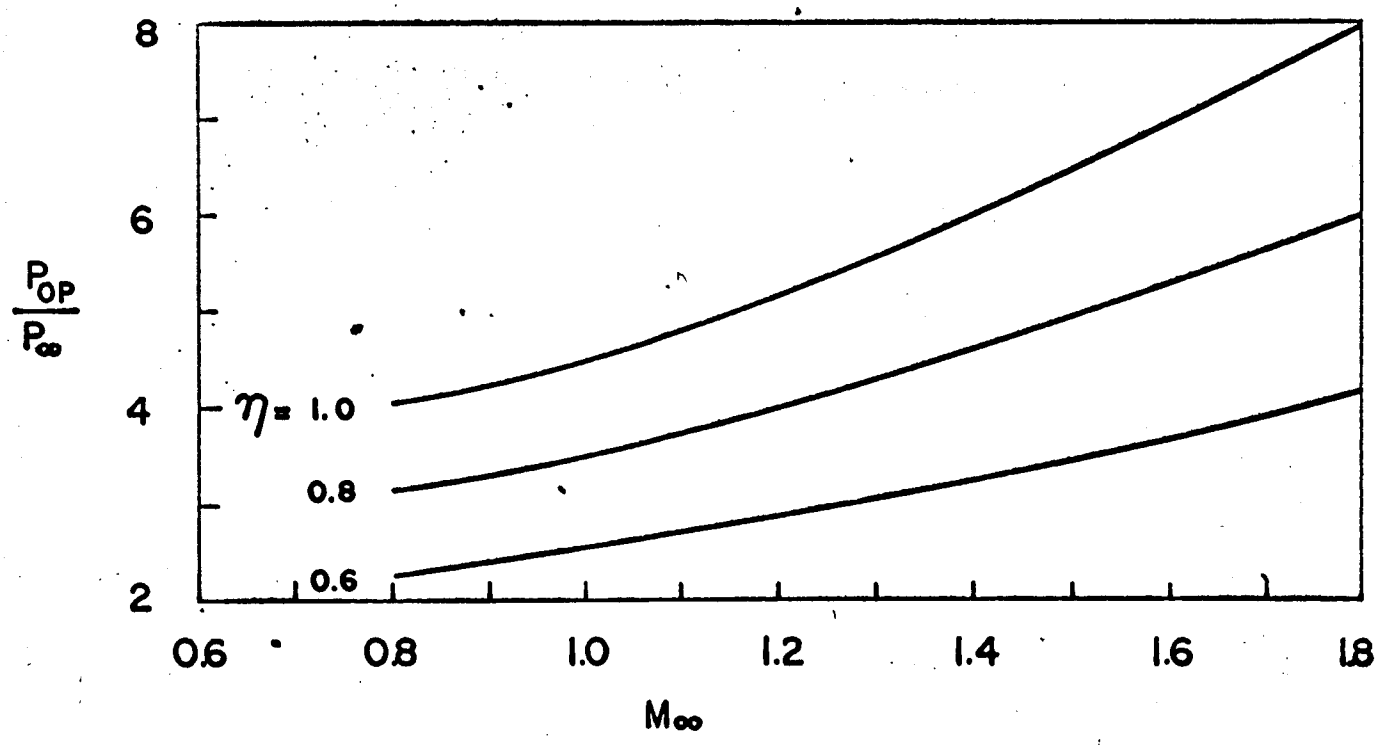

FIG. 10 THEORETICAL IN-FLIGHT P_{OP} / P_∞ SCHEDULE BASED ON AN EJECTOR OPERATING POINT AS AFFECTED BY INTAKE EFFICIENCY

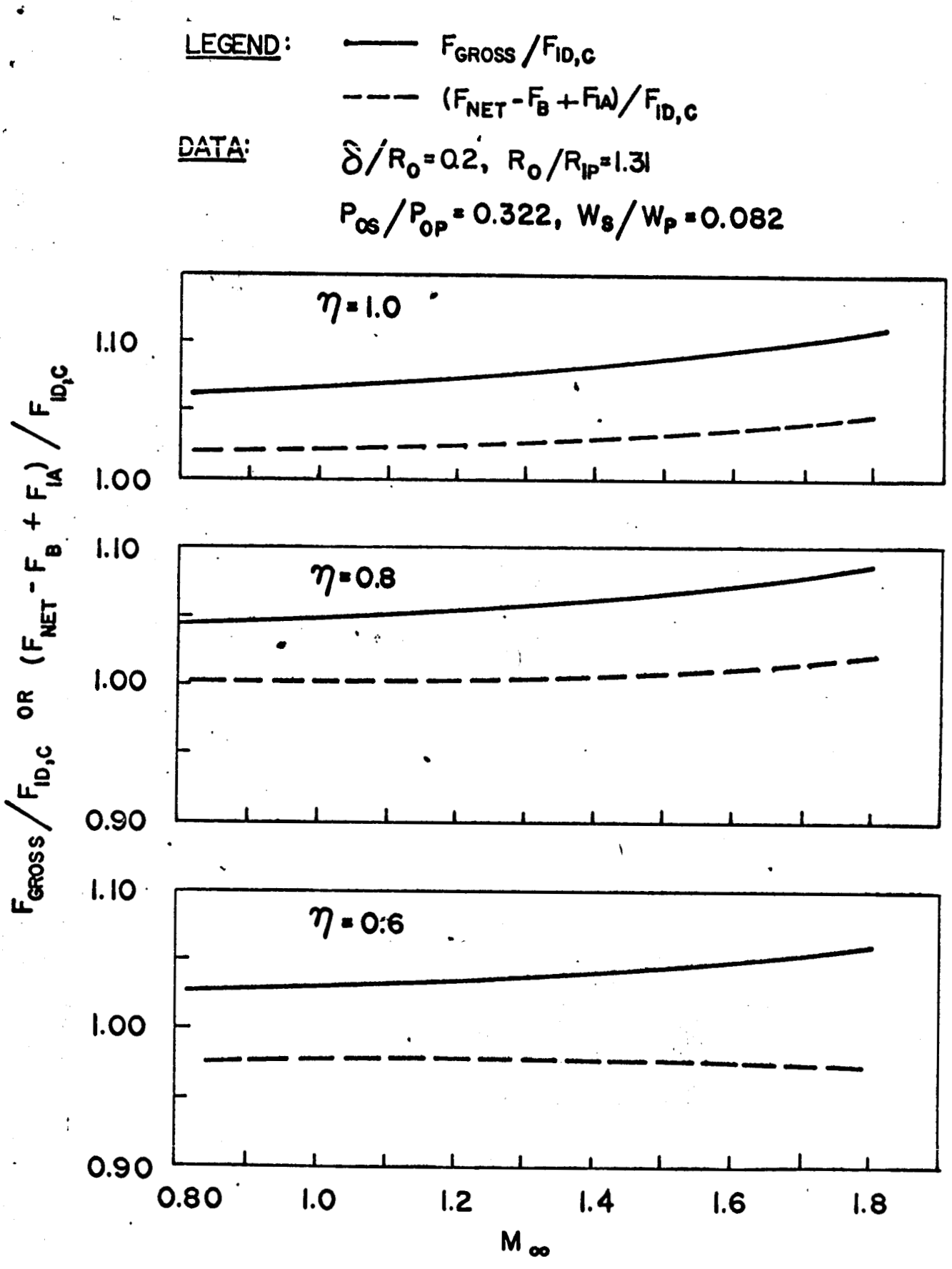

FIG. 11 THEORETICAL IN-FLIGHT THRUST CHARACTERISTICS FOR ONE EJECTOR OPERATING POINT AS AFFECTED BY INTAKE EFFICIENCY (REFERENCED TO AN IDEAL CONVERGING NOZZLE)

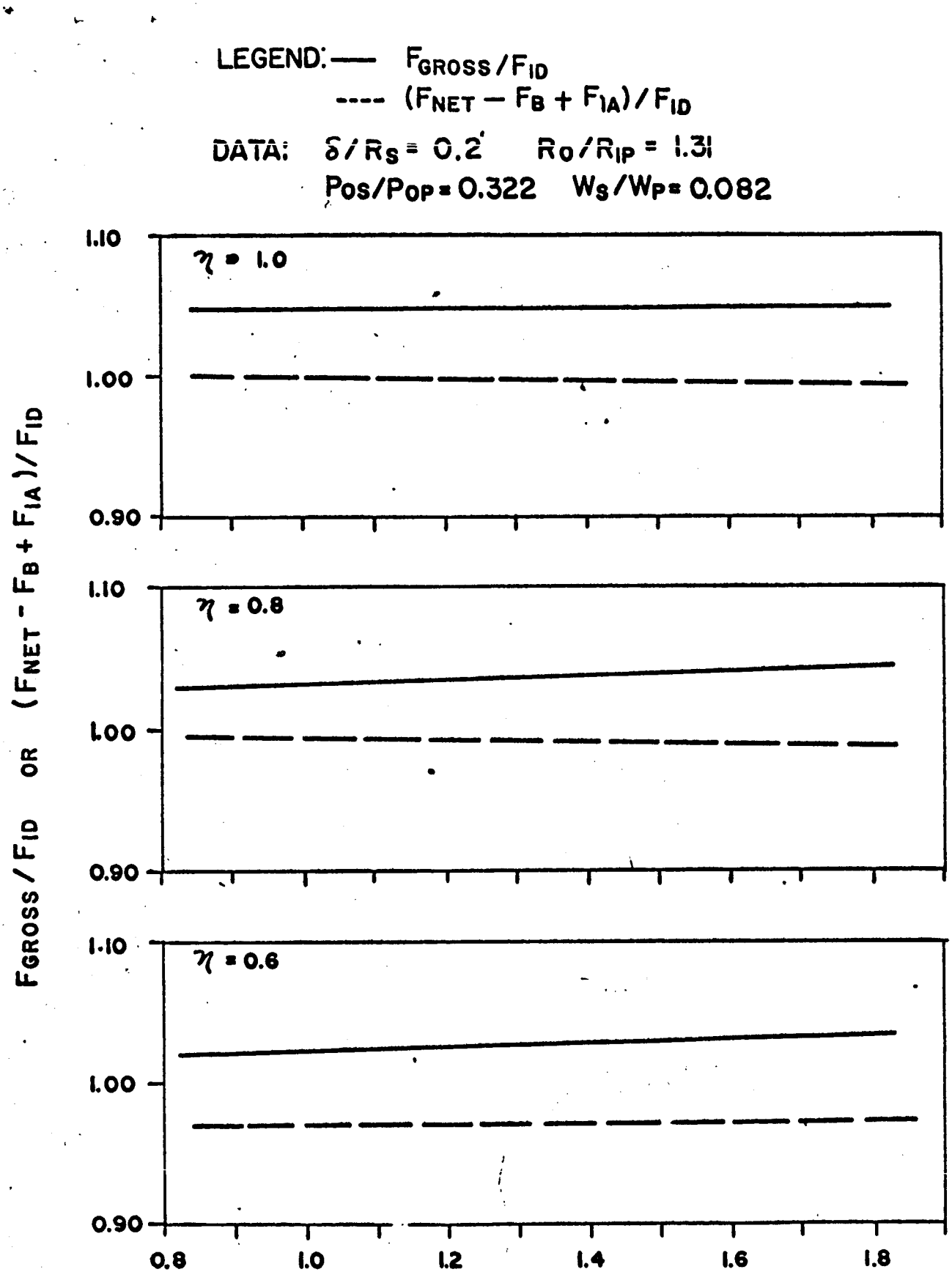

FIG. 12 THEORETICAL IN-FLIGHT THRUST CHARACTERISTICS FOR ONE EJECTOR OPERATING POINT AS AFFECTED BY INTAKE EFFICIENCY (REFERENCED TO AN IDEAL FULLY EXPANDED NOZZLE)

	INPUT DATA
1.	EJECTOR GEOMETRY
2.	PRIMARY GAS AND FLOW CONDITION (K_P & M_{IP})
3.	SECONDARY GAS (K_S)
	CALCULATION PARAMETER
1.	PRESSURE RATIO (P_{IS}/P_{OP})
	(WITH VARIABLE M_{IS} THIS YIELDS P_{OS}/P_{OP})
	VARIABLE
1.	INITIAL SECONDARY MACH NO. (M_{IS})
	(EQUIVALENT TO W_S/W_P)
	SOLUTION OUTPUT DATA
1.	$M_{IS} \leq 1$ AND W_S/W_P
2.	INFORMATION ABOUT JET BOUNDARY, e.g., $R_P(z)$
3.	WALL PRESSURE DISTRIBUTION, $P_W(z)$
4.	PRESSURE – AREA INTEGRAL ON SHROUD

TABLE I. ESSENTIAL CHARACTERISTICS OF INVISCID EJECTOR COMPUTER PROGRAM (7094 IBM SYSTEM)